A Constraint-Based Approach to Rigid Body Dynamics for Virtual Reality Applications

Jörg Sauer
Daimler-Benz AG
Research and Technology
P.O.Box 2360
D-89013 Ulm
Germany
email: sauer@dbag.ulm.DaimlerBenz.COM

Elmar Schömer
Universität des Saarlandes
Lehrstuhl Prof. Hotz
Im Stadtwald
D-66123 Saarbrücken
Germany
email: schoemer@cs.uni-sb.de

Abstract

The GALILEO-system is a developmental state-of-the-art rigid body simulation tool with a strong bias to the simulation of unilateral contacts for virtual reality applications. On the one hand the system is aimed at closing the gap between the 'paradigms of impulse-based simulation' and of 'constraint-based simulation'. On the other hand the chosen simulation techniques enable a balancing of the trade-off between the real-time demands of virtual environments (i.e. 15-25 visualizations per second) and the degree of physical correctness of the simulation. The focus of this paper lies on the constraint-based simulation approach to three-dimensional multibody systems including a scalable friction model. This is only one of the two main components of the GALILEO-software-module. A nonlinear complementarity problem (NCP) describes the equations of motion, the contact conditions of the objects and the Coulomb friction model. Further on we show, as an interesting evaluation example from the field of 'classical mechanics', the first rigid body simulation of the tippe-top.

1 Introduction

We believe virtual reality (VR) to be one of the 'leading-edge' technologies of the next decade that will have a significant impact on animation and simulation. The physical modeling of virtual objects and based on it the simulation of rigid body dynamics in virtual environments will play a very important role throughout the whole manufacturing- and engineering-industry. No matter whether automotive, aircraft or railway industry, simulation in the early product development cycles becomes more and more important. That already is our experience at the Virtual Reality Competence Center (VRCC) of Daimler-Benz Research. Virtual Reality helps to shorten product development times and therefore cuts costs. In the following we present the design of our state-of-the-art system for the real-time simulation of three-dimensional multibody problems in the presence of sticking-, sliding- and rolling-friction (see also [SS98]).

Contact situations in virtual worlds could generally be classified according to figure 1:

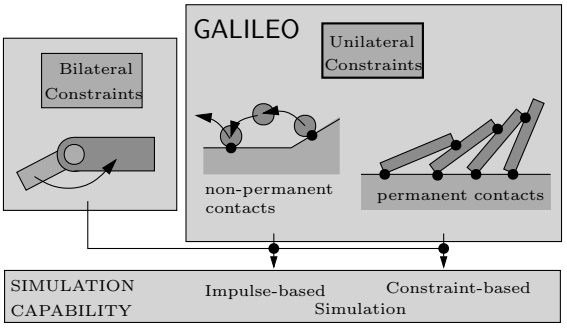

Figure 1: The classification of contact situations.

In the GALILEO-module (that is part of the VR-software-platform DBView developed at the VRCC) we concentrate on unilateral contact situations, although the approaches would also be appropriate for the simulation of bilateral contact situations. The impulse-based technique due to Mirtich and Canny ([MC94], [MC95]), that is itself based on Stronge ([St90], [St91]), Keller [Ke86] and Hahn [Ha88], is especially suitable for the simulation of temporary contacts at one contact point. We reimplemented their approach. The constraint-based technique is based on a work of Stewart and Trinkle [ST95], who themselves developed further [Mo86] and [MM93]. It rather is a simulation approach for problems with multiple (permanent) contacts between multiple objects. Former work in the computer graphics community is from Moore and Wilhelms [MW88], Barzel and Barr [BB88], Witkin, Gleicher and Welch [WGW90] and especially from Baraff ([Ba89], see [Ba93] for an overview of his early work). One of the great open problems in the field of rigid body simulation, as also formulated by Mirtich in his Ph.D.-thesis [Mi96], is the design and implementation of a hybrid simulation system that combines both types of simulation paradigms. The solution of this problem is the long-term scientific objective of the GALILEO-simulation environment. The above distinction of the techniques is not only justified by the observation of the occurring real contact situations, but also by the fact, that for one contact point configurations a 'physically much more correct modeling' is possible than for the multibody problems. (See classical problems: energy-dissipation, transition from static to dynamic friction, paradoxa of Painlevé, static indeterminacy,

jamming and wedging etc.).

In the following section we present the constraint-based approach, which provides an iterative solution of linear complementarity problems, and we evaluate the simulation technique with an example from the field of classical dynamics. The simulation of the tippe-top shows the physical modeling capabilities of the approach and especially the advantages of the scalable friction model. Because of the real-time demands of virtual reality applications a scalable friction model for time-critical computing is of utmost importance. The simulation of mechanical configurations with unilateral contacts is very useful in the industrial field e.g. when it comes to the simulation of fitting-operations in engine-design. Beyond that the physically correct behaviour of objects in virtual worlds helps to increase the feeling of immersion for the user.

2 The constraint-based approach

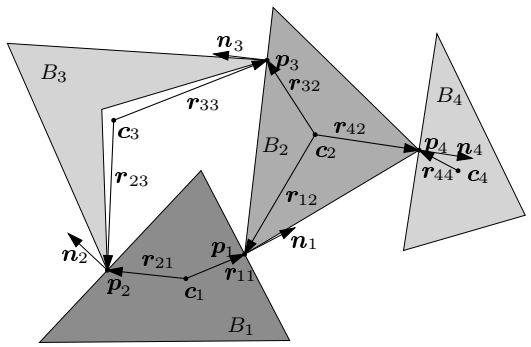

Figure 2: A two-dimensional multibody system example.

The virtual objects either behave according to the laws of Newtonian physics or they are interactively moved by a user with e.g. a space-mouse or a data-glove. In both cases the current contact points and the geometrical and dynamical configurations of the objects in contact serve as an input to the algorithm in every frame of the simulation. The provision of this information is guaranteed by the interplay of the collision detection with the dynamics simulation module. Therefore our approach is suitable for a physical modeling of virtual worlds as well as for animation purposes or interactively specified object behaviour.

2.1 The frictionless case

For reasons of simplicity we assume in our first approach that there is no friction. Suppose the multibody system has n objects in mutual contact at K contact points as in figure 2. The geometric configuration is described by a contact data table:

k	i_k	j_k	$\boldsymbol{n}_k$	$\boldsymbol{p}_k$
1	1	2	·	·
2	1	3	·	·
3	2	3	·	·
4	2	4	·	·

For the k-th contact point the normal vector $\boldsymbol{n}_k$ is directed from the contact object with the smaller index to the contact object with the larger index: if the normal is directed from B_{i_k} to B_{j_k}, then $i_k < j_k$ with $1 \le i_k, j_k \le n$. $\boldsymbol{p}_k$ denotes the vector to the k-th contact point and f_k is the magnitude of the contact force acting in direction $\boldsymbol{n}_k$ in the absence of friction. $\boldsymbol{r}_{kl} = \boldsymbol{p}_k - \boldsymbol{c}_l$ points from the center of mass of object B_l $(l = 1, \ldots, n)$ to the k-th contact point. $\boldsymbol{q}_l$ is the orientation of object B_l described as a quaternion. If the object B_l is fixed in space, then for its mass holds $m_l = \infty$, its inertia matrix is $\mathbf{I}_l = \infty\mathbf{E}$ and the velocities are $\boldsymbol{v}_l = \boldsymbol{\omega}_l = \mathbf{0}$. $\mathbf{E} \in \mathbb{R}^{3\times3}$ is the identity matrix. The generalized Newton-Euler equations of motion for the objects B_l and $\boldsymbol{F}_k := f_k\boldsymbol{n}_k$ are:

$$
\begin{aligned}
\dot{\boldsymbol{c}}_l &= \boldsymbol{v}_l, \\
\dot{\boldsymbol{q}}_l &= \frac{1}{2}\boldsymbol{\omega}_l\boldsymbol{q}_l \quad \text{(quaternion multiplication)}, \\
\dot{\boldsymbol{v}}_l &= m_l^{-1}\sum_{\{k|j_k=l\}}\boldsymbol{F}_k - m_l^{-1}\sum_{\{k|i_k=l\}}\boldsymbol{F}_k + \boldsymbol{g}, \\
\dot{\boldsymbol{\omega}}_l &= \mathbf{I}_l^{-1}\sum_{\{k|j_k=l\}}\boldsymbol{r}_{kl}\times\boldsymbol{F}_k - \mathbf{I}_l^{-1}\sum_{\{k|i_k=l\}}\boldsymbol{r}_{kl}\times\boldsymbol{F}_k - \mathbf{I}_l^{-1}\boldsymbol{\omega}_l\times\mathbf{I}_l\boldsymbol{\omega}_l
\end{aligned}
$$

Our objective is to determine the constraint-forces $\boldsymbol{F}_k$ for $k = 1, \ldots, K$. To give up the component-wise description the following vectors and matrices are quite useful: The generalized velocity vector $\boldsymbol{u} \in \mathbb{R}^{6n}$

$$\boldsymbol{u} = [\boldsymbol{v}_1, \boldsymbol{\omega}_1, \ldots, \boldsymbol{v}_n, \boldsymbol{\omega}_n]^T,$$

the generalized position and orientation vector $\boldsymbol{s} \in \mathbb{R}^{7n}$

$$\boldsymbol{s} = [\boldsymbol{c}_1, \boldsymbol{q}_1, \ldots, \boldsymbol{c}_n, \boldsymbol{q}_n]^T,$$

the vector of the magnitudes of the contact forces $\boldsymbol{f} \in \mathbb{R}^{K}$

$$\boldsymbol{f} = [f_1, f_2, \ldots, f_K]^T,$$

the vector of external forces $\boldsymbol{f}_{ext} \in \mathbb{R}^{6n}$

$$\boldsymbol{f}_{ext} = [m_1\boldsymbol{g}, -\boldsymbol{\omega}_1\times\mathbf{I}_1\boldsymbol{\omega}_1, \ldots, m_n\boldsymbol{g}, -\boldsymbol{\omega}_n\times\mathbf{I}_n\boldsymbol{\omega}_n]^T,$$

the matrix $\mathbf{S} \in \mathbb{R}^{7n\times6n}$

$$\mathbf{S} = \begin{bmatrix} \mathbf{E} & & & \mathbf{0} \\ & \mathbf{Q}_1 & & \\ & & \ddots & \\ & & & \mathbf{E} \\ \mathbf{0} & & & \mathbf{Q}_n \end{bmatrix}$$

with $\boldsymbol{q}_l := [q_{l0}, \ldots, q_{l3}]^T \in \mathbb{R}^4$ and $\mathbf{Q}_l \in \mathbb{R}^{4\times3}$

$$\mathbf{Q}_l = \frac{1}{2}\begin{bmatrix} -q_{l1} & -q_{l2} & -q_{l3} \\ q_{l0} & q_{l3} & -q_{l1} \\ -q_{l3} & q_{l0} & q_{l2} \\ q_{l2} & -q_{l1} & q_{l0} \end{bmatrix},$$

the generalized mass matrix $\mathbf{M} \in \mathbb{R}^{6n\times6n}$

$$\mathbf{M} = \begin{bmatrix} m_1\mathbf{E} & & & \mathbf{0} \\ & \mathbf{I}_1 & & \\ & & \ddots & \\ & & & m_n\mathbf{E} \\ \mathbf{0} & & & \mathbf{I}_n \end{bmatrix},$$

the matrix of contact normals $\mathbf{N} \in \mathbb{R}^{3K\times K}$

$$\mathbf{N} = \begin{bmatrix} \boldsymbol{n}_1 & & \mathbf{0} \\ & \boldsymbol{n}_2 & \\ & & \ddots \\ \mathbf{0} & & \boldsymbol{n}_K \end{bmatrix},$$

and the matrix of contact conditions $\mathbf{J} \in \mathbb{R}^{6n \times 3K}$

$$\mathbf{J}_{lk} = \begin{cases} -\mathbf{E} & \text{for } l = 2i_k - 1 \\ -\mathbf{r}^{\times}_{ki_k} & \text{for } l = 2i_k \\ \mathbf{E} & \text{for } l = 2j_k - 1 \\ \mathbf{r}^{\times}_{kj_k} & \text{for } l = 2j_k \\ \mathbf{0} & \text{in all other cases} \end{cases} .$$

$\mathbf{r}^{\times} \in \mathbb{R}^{3\times 3}$ is the skew-symmetric matrix

$$\mathbf{r}^{\times} = \begin{bmatrix} 0 & -r_3 & r_2 \\ r_3 & 0 & -r_1 \\ -r_2 & r_1 & 0 \end{bmatrix}$$

with $\mathbf{r}^{\times}\boldsymbol{a} = \boldsymbol{r} \times \boldsymbol{a}$ for $\boldsymbol{a} \in \mathbb{R}^3$. Every column of the matrix $\mathbf{J}$ corresponds to one contact point and every row to one object. The column of every contact point contains two displacement vectors $\boldsymbol{r}$ for the objects in contact. The transposed matrix $\mathbf{J}^T$ has the following structure indicated by its k-th row:

$$\begin{bmatrix} & & \overset{2i_k-1}{\downarrow} & \overset{2i_k}{\downarrow} & & & \overset{2j_k-1}{\downarrow} & \overset{2j_k}{\downarrow} & \\ \mathbf{0}\ldots\mathbf{0} & & -\mathbf{E} & \mathbf{r}^{\times}_{ki_k} & \mathbf{0}\ldots\mathbf{0} & & \mathbf{E} & -\mathbf{r}^{\times}_{kj_k} & \mathbf{0}\ldots\mathbf{0} \end{bmatrix} \leftarrow k$$

Further on we need the projection-matrix $\mathbf{P}_k \in \mathbb{R}^{3K\times 3}$, whose transposed matrix looks like:

$$\mathbf{P}_k^T = \begin{bmatrix} & & \overset{k}{\downarrow} & & \\ \mathbf{0}\ldots\mathbf{0} & & \mathbf{E} & & \mathbf{0}\ldots\mathbf{0} \end{bmatrix} .$$

The projection-matrix enables us to extract the contact configuration of two objects at their contact point from the matrix of contact conditions $\mathbf{J}$. Using this notation the equations of motion can be formulated in their continuous and discretized (Euler-scheme) version:

$$\begin{aligned} \dot{\boldsymbol{s}} &= \mathbf{S}\boldsymbol{u} \\ \dot{\boldsymbol{u}} &= \mathbf{M}^{-1}(\mathbf{J}\mathbf{N}\boldsymbol{f} + \boldsymbol{f}_{ext}) \\ \Rightarrow \quad \boldsymbol{s}^{t+\Delta t} &= \boldsymbol{s}^t + \Delta t \mathbf{S}\boldsymbol{u}^{t+\Delta t} \qquad (1) \\ \boldsymbol{u}^{t+\Delta t} &= \boldsymbol{u}^t + \Delta t \mathbf{M}^{-1}(\mathbf{J}\mathbf{N}\boldsymbol{f} + \boldsymbol{f}_{ext}) . \qquad (2) \end{aligned}$$

The normal component of the relative contact velocity of the k-th contact point is given by:

$$\begin{aligned} \boldsymbol{n}_k^T \mathbf{P}_k^T \mathbf{J}^T \boldsymbol{u} &= \boldsymbol{n}_k^T(\boldsymbol{v}_{j_k} + \boldsymbol{\omega}_{j_k} \times \boldsymbol{r}_{kj_k}) \\ &- \boldsymbol{n}_k^T(\boldsymbol{v}_{i_k} + \boldsymbol{\omega}_{i_k} \times \boldsymbol{r}_{ki_k}) . \end{aligned}$$

If body B_{i_k} and B_{j_k} already touch at contact point $\boldsymbol{p}_k$ at time t for the velocities $\boldsymbol{u}^{t+\Delta t}$ the complementarity condition

$$\boldsymbol{n}_k^T \mathbf{P}_k^T \mathbf{J}^T \boldsymbol{u}^{t+\Delta t} \geq 0 \quad \text{compl. to} \quad f_k \geq 0$$

must hold. Note that '$\boldsymbol{a}$ compl. to $\boldsymbol{b}$' is equivalent to $\boldsymbol{a}^T\boldsymbol{b} = 0$ for $\boldsymbol{a}, \boldsymbol{b} \in \mathbb{R}^{\mathrm{d}}$. If there is no contact at the potential contact point $\boldsymbol{p}_k$ at time t, the following linearized complementarity condition can be used:

$$\boldsymbol{n}_k^T \mathbf{P}_k^T \mathbf{J}^T \boldsymbol{u}^{t+\Delta t} \geq \frac{\nu_k}{\Delta t} \quad \text{compl. to} \quad f_k \geq 0 .$$

The linearization process that determines ν_k will be explained more detailed in section 2.4. Formulated for all contacts the condition reads as:

$$\mathbf{N}^T \mathbf{J}^T \boldsymbol{u}^{t+\Delta t} \geq \frac{\boldsymbol{\nu}}{\Delta t} \quad \text{compl. to} \quad \boldsymbol{f} \geq \mathbf{0} \qquad (3)$$

with $\boldsymbol{\nu} = [\nu_1, \ldots, \nu_K]^T \in \mathbb{R}^{\mathrm{K}}$ and $\mathbf{0} = [0, \ldots, 0]^T \in \mathbb{R}^{\mathrm{K}}$. We insert equation (2) into equation (3) and obtain:

$$\mathbf{N}^T \mathbf{J}^T \mathbf{M}^{-1} \mathbf{J}\mathbf{N} \Delta t \boldsymbol{f} + \mathbf{N}^T \mathbf{J}^T (\boldsymbol{u}^t + \Delta t \mathbf{M}^{-1} \boldsymbol{f}_{ext}) - \frac{\boldsymbol{\nu}}{\Delta t} \geq \mathbf{0} .$$

This is a linear complementarity problem (LCP) of the form

$$\mathbf{A}\boldsymbol{x} + \boldsymbol{b} \geq \mathbf{0} \quad \text{compl. to} \quad \boldsymbol{x} \geq \mathbf{0}$$

with $\mathbf{A} \in \mathbb{R}^{\mathrm{K}\times\mathrm{K}}$ and $\boldsymbol{x}, \boldsymbol{b} \in \mathbb{R}^{\mathrm{K}}$. It can be solved with the classical Lemke-algorithm as e.g. described in the monograph [CPS92]. We now describe the structure of the matrix

$$\mathbf{A} = \mathbf{N}^T \mathbf{J}^T \mathbf{M}^{-1} \mathbf{J}\mathbf{N}$$

in more detail. It is symmetric and positive definite, because the generalized mass matrix $\mathbf{M}$ has these properties. The elements of $\mathbf{A}$ are

$$\begin{aligned} \mathbf{A}_{lk} &= \delta_{i_l i_k} \boldsymbol{n}_l^T \left(\frac{1}{m_{i_k}} \mathbf{E} - \mathbf{r}^{\times}_{li_l} \mathbf{I}^{-1}_{i_k} \mathbf{r}^{\times}_{ki_k} \right) \boldsymbol{n}_k \\ &- \delta_{i_l j_k} \boldsymbol{n}_l^T \left(\frac{1}{m_{j_k}} \mathbf{E} - \mathbf{r}^{\times}_{li_l} \mathbf{I}^{-1}_{j_k} \mathbf{r}^{\times}_{kj_k} \right) \boldsymbol{n}_k \\ &- \delta_{j_l i_k} \boldsymbol{n}_l^T \left(\frac{1}{m_{i_k}} \mathbf{E} - \mathbf{r}^{\times}_{lj_l} \mathbf{I}^{-1}_{i_k} \mathbf{r}^{\times}_{ki_k} \right) \boldsymbol{n}_k \\ &+ \delta_{j_l j_k} \boldsymbol{n}_l^T \left(\frac{1}{m_{j_k}} \mathbf{E} - \mathbf{r}^{\times}_{lj_l} \mathbf{I}^{-1}_{j_k} \mathbf{r}^{\times}_{kj_k} \right) \boldsymbol{n}_k \end{aligned}$$

with the Kronecker-symbol being

$$\delta_{ij} = \begin{cases} 1 & \text{for } i = j \\ 0 & \text{for } i \neq j \end{cases} .$$

The structure of matrix $\mathbf{A}$ reflects the adjacency matrix

$$\begin{bmatrix} 1 & 1 & 1 & 1 \\ 1 & 1 & 1 & 0 \\ 1 & 1 & 1 & 1 \\ 1 & 0 & 1 & 1 \end{bmatrix}$$

of the dual undirected graph of mutual body contacts. Because two objects can touch at more than one contact point also multiple edges between two nodes in the graph are possible. Now we consider the multibody problem in the presence of Coulomb friction.

2.2 The friction case

In order to obtain a linear complementarity problem again, we linearize the Coulomb friction cone at contact points by using a standard technique. In addition to the normal vector $\boldsymbol{n}_k$, we define two vectors $\boldsymbol{t}_{k1}$ and $\boldsymbol{t}_{k2}$ that span the tangential plane at the k-th contact point. The three vectors build up an orthonormal system. The friction cone at the contact point is discretized with a number of $\eta = 2i$ ($i \in \mathbb{N}, i \geq 2$) direction vectors $\boldsymbol{d}_{kh}$ ($h = 1, \ldots, \eta$) as follows:

$$\begin{aligned} \mathbf{D}_k &= [\boldsymbol{d}_{k1}, \ldots, \boldsymbol{d}_{k\eta}] \in \mathbb{R}^{3\times\eta}, \\ \boldsymbol{d}_{kh} &= \cos\frac{2(h-1)\pi}{\eta} \boldsymbol{t}_{k1} + \sin\frac{2(h-1)\pi}{\eta} \boldsymbol{t}_{k2} \end{aligned}$$

Thus we obtain a friction pyramid with η facets, for further explanation see figure 3.

β_{kh} is the component of the friction force in direction $\boldsymbol{d}_{kh}$ and all these components build up the vector $\boldsymbol{\beta}_k$ =

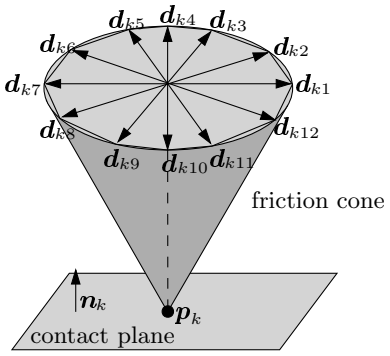

Figure 3: The friction cone and the corresponding friction pyramid with $\eta = 12$ facets in the case of a contact between two objects at contact point $\boldsymbol{p}_k$.

$[\beta_{k1}, \beta_{k2}, \ldots, \beta_{k\eta}]^T \in \mathbb{R}^\eta$. The equations of motion are the same ones as before, but now $\boldsymbol{F}_k$ is defined as $f_k \boldsymbol{n}_k + \mathbf{D}_k \boldsymbol{\beta}_k$. Using the abbreviations $\boldsymbol{\beta} = [\boldsymbol{\beta}_1, \boldsymbol{\beta}_2, \ldots, \boldsymbol{\beta}_K]^T \in \mathbb{R}^{\eta \cdot \mathrm{K}}$ and

$$\mathbf{D} = \begin{bmatrix} \mathbf{D}_1 & & & \\ & \mathbf{D}_2 & & \\ & & \ddots & \\ & & & \mathbf{D}_K \end{bmatrix} \in \mathbb{R}^{3\mathrm{K} \times \eta \cdot \mathrm{K}},$$

the generalized acceleration is again described by the Newton-Euler equations:

$$\begin{aligned} \dot{\boldsymbol{u}} &= \mathbf{M}^{-1}(\mathbf{J}(\mathbf{N}\boldsymbol{f} + \mathbf{D}\boldsymbol{\beta}) + \boldsymbol{f}_{ext}) \\ \Rightarrow \quad \boldsymbol{u}^{t+\Delta t} &= \boldsymbol{u}^t + \Delta t \mathbf{M}^{-1}(\mathbf{J}(\mathbf{N}\boldsymbol{f} + \mathbf{D}\boldsymbol{\beta}) + \boldsymbol{f}_{ext}) \quad (4) \end{aligned}$$

At the k-th contact point, the following complementarity conditions must hold:

$$\lambda_k \boldsymbol{e}_k + \mathbf{D}_k^T \mathbf{P}_k^T \mathbf{J}^T \boldsymbol{u}^{t+\Delta t} \geq \mathbf{0} \quad \text{compl. to} \quad \boldsymbol{\beta}_k \geq \mathbf{0}\,, \quad (5)$$

$$\mu_k f_k - \boldsymbol{e}_k^T \boldsymbol{\beta}_k \geq 0 \quad \text{compl. to} \quad \lambda_k \geq 0\,, \quad (6)$$

$$\boldsymbol{n}_k^T \mathbf{P}_k^T \mathbf{J}^T \boldsymbol{u}^{t+\Delta t} - \frac{\nu_k}{\Delta t} \geq 0 \quad \text{compl. to} \quad f_k \geq 0\,. \quad (7)$$

$\boldsymbol{e}_k = [1, \ldots, 1]^T \in \mathbb{R}^\eta$ and μ_k is the friction coefficient at the k-th contact point. λ_k has no physical meaning, but it is in most cases an approximation to the magnitude of the relative contact velocity. The Coulomb law distinguishes two different cases:

1. sliding (dynamic) friction:

$$\dot{\boldsymbol{p}}_t \neq 0 \quad \Rightarrow \quad \boldsymbol{F}_t = -\mu |\boldsymbol{F}_n| \frac{\dot{\boldsymbol{p}}_t}{|\dot{\boldsymbol{p}}_t|},$$

2. sticking (static) friction:

$$\dot{\boldsymbol{p}}_t = 0 \quad \Rightarrow \quad |\boldsymbol{F}_t| \leq \mu |\boldsymbol{F}_n|\,.$$

$\mu \in [0, 1]$ is the friction coefficient, $\dot{\boldsymbol{p}}_t$ is the relative velocity of the contact point $\boldsymbol{p}$ in the contact plane, $\boldsymbol{F}_t$ is the contact force in tangential direction and $\boldsymbol{F}_n$ in normal direction. These two cases are approximately represented in the complementarity conditions (5) and (6). For further details see the work of Stewart and Trinkle. The vector $\mathbf{D}_k^T \mathbf{P}_k^T \mathbf{J}^T \boldsymbol{u}^{t+\Delta t}$ in (5) describes the relative contact velocities in the directions $\boldsymbol{d}_{k1}, \ldots, \boldsymbol{d}_{k\eta}$. To eliminate $\boldsymbol{u}^{t+\Delta t}$ we insert equation (4) into the inequations of (5) and (7) and obtain instead of the complementarity conditions (5) and (7) as new conditions for the k-th contact point:

$$\begin{aligned} & \Delta t \mathbf{D}_k^T \mathbf{P}_k^T \mathbf{J}^T \mathbf{M}^{-1} \mathbf{J} \mathbf{D} \boldsymbol{\beta} + \Delta t \mathbf{D}_k^T \mathbf{P}_k^T \mathbf{J}^T \mathbf{M}^{-1} \mathbf{J} \mathbf{N} \boldsymbol{f} \quad (8) \\ + \quad & \lambda_k \boldsymbol{e}_k + \mathbf{D}_k^T \mathbf{P}_k^T \mathbf{J}^T \boldsymbol{u}^t + \Delta t \mathbf{D}_k^T \mathbf{P}_k^T \mathbf{J}^T \mathbf{M}^{-1} \boldsymbol{f}_{ext} \geq \mathbf{0} \\ & \text{compl. to} \quad \boldsymbol{\beta}_k \geq \mathbf{0}\,, \\ & \Delta t \boldsymbol{n}_k^T \mathbf{P}_k^T \mathbf{J}^T \mathbf{M}^{-1} \mathbf{J} \mathbf{D} \boldsymbol{\beta} + \Delta t \boldsymbol{n}_k^T \mathbf{P}_k^T \mathbf{J}^T \mathbf{M}^{-1} \mathbf{J} \mathbf{N} \boldsymbol{f} \quad (9) \\ + \quad & \boldsymbol{n}_k^T \mathbf{P}_k^T \mathbf{J}^T \boldsymbol{u}^t + \Delta t \boldsymbol{n}_k^T \mathbf{P}_k^T \mathbf{J}^T \mathbf{M}^{-1} \boldsymbol{f}_{ext} - \tfrac{\nu_k}{\Delta t} \geq 0 \\ & \text{compl. to} \quad f_k \geq 0\,. \end{aligned}$$

By rearranging the complementarity conditions (6), (8) and (9), the LCP-formulation is built up again:

$$\begin{bmatrix} \mathbf{D}^T \mathbf{J}^T \mathbf{M}^{-1} \mathbf{J} \mathbf{D} & \mathbf{D}^T \mathbf{J}^T \mathbf{M}^{-1} \mathbf{J} \mathbf{N} & \mathbf{e} \\ \mathbf{N}^T \mathbf{J}^T \mathbf{M}^{-1} \mathbf{J} \mathbf{D} & \mathbf{N}^T \mathbf{J}^T \mathbf{M}^{-1} \mathbf{J} \mathbf{N} & \mathbf{0} \\ -\mathbf{e}^T & \boldsymbol{\mu} & \mathbf{0} \end{bmatrix} \cdot \begin{bmatrix} \Delta t \boldsymbol{\beta} \\ \Delta t \boldsymbol{f} \\ \boldsymbol{\lambda} \end{bmatrix}$$

$$+ \quad \begin{bmatrix} \mathbf{D}^T \mathbf{J}^T (\boldsymbol{u}^t + \Delta t \mathbf{M}^{-1} \boldsymbol{f}_{ext}) \\ \mathbf{N}^T \mathbf{J}^T (\boldsymbol{u}^t + \Delta t \mathbf{M}^{-1} \boldsymbol{f}_{ext}) - \frac{\boldsymbol{\nu}}{\Delta t} \\ 0 \end{bmatrix} \geq \mathbf{0}$$

$$\text{complementary to} \begin{bmatrix} \Delta t \boldsymbol{\beta} \\ \Delta t \boldsymbol{f} \\ \boldsymbol{\lambda} \end{bmatrix} \geq \mathbf{0}.$$

$\boldsymbol{\mu} \in \mathbb{R}^{\mathrm{K} \times \mathrm{K}}$, $\boldsymbol{\lambda} \in \mathbb{R}^{\mathrm{K} \times \mathrm{K}}$ and $\mathbf{e} \in \mathbb{R}^{\eta \cdot \mathrm{K} \times \mathrm{K}}$ denote diagonal-matrices. The matrix $\mathbf{A}$ of the above LCP $\mathbf{A}\boldsymbol{x} + \boldsymbol{b} \geq \mathbf{0}$ has the structure shown in figure 4.

$$\mathbf{A} = \left[\begin{array}{ccccccc} \mathbf{A_{11}} & \cdots & \mathbf{A_{1K}} & \boldsymbol{a}_{11} & \cdots & \boldsymbol{a}_{1K} & \boldsymbol{e}_1 \quad \boldsymbol{o} \\ \vdots & \ddots & \vdots & \vdots & & \vdots & \\ \mathbf{A_{1K}^T} & \cdots & \mathbf{A_{KK}} & \boldsymbol{a}_{K1} & \cdots & \boldsymbol{a}_{KK} & \boldsymbol{o} \quad \boldsymbol{e}_K \\ \boldsymbol{a}_{11}^T & \cdots & \boldsymbol{a}_{K1}^T & \multicolumn{3}{c}{\multirow{2}{*}{$\mathbf{A_{00}}$}} & \multirow{2}{*}{$\mathbf{O}$} \\ \vdots & & \vdots & & & & \\ \boldsymbol{a}_{1K}^T & \cdots & \boldsymbol{a}_{KK}^T & & & & \\ \boldsymbol{e}_1^T & & \boldsymbol{o}^T & \multicolumn{3}{c}{\multirow{2}{*}{$\boldsymbol{\mu}$}} & \multirow{2}{*}{$\mathbf{O}$} \\ & \ddots & & & & & \\ \boldsymbol{o}^T & & \boldsymbol{e}_K^T & & & & \end{array}\right]$$

Figure 4: The structure of matrix $\mathbf{A}$.

A detailed analysis of the matrix $\mathbf{A}$ and the vector $\boldsymbol{b}$ enables us to efficiently fill them component-wise in every iteration of the fixpoint-iteration described in section 2.3. $\mathbf{A} \in \mathbb{R}^{(\eta+2) \cdot \mathrm{K} \times (\eta+2) \cdot \mathrm{K}}$ because $\mathbf{A}_{lk} \in \mathbb{R}^{\eta \times \eta}$ and $\boldsymbol{a}_{lk} \in \mathbb{R}^\eta$ for $1 \leq l, k \leq K$, $\mathbf{A}_{00} \in \mathbb{R}^{\mathrm{K} \times \mathrm{K}}$, the zero matrix $\mathbf{O} \in \mathbb{R}^{\mathrm{K} \times \mathrm{K}}$ and $\boldsymbol{e}_k, \mathbf{0} \in \mathbb{R}^\eta$ for $1 \leq k \leq K$. For $1 \leq l, k \leq K$ holds:

$$\begin{aligned} \mathbf{A}_{00} &= \mathbf{N}^T \mathbf{J}^T \mathbf{M}^{-1} \mathbf{J} \mathbf{N}, \\ \mathbf{A}_{lk} &= \mathbf{D}_l^T \mathbf{P}_l^T \mathbf{J}^T \mathbf{M}^{-1} \mathbf{J} \mathbf{P}_k \mathbf{D}_k, \\ \boldsymbol{a}_{lk} &= \mathbf{D}_l^T \mathbf{P}_l^T \mathbf{J}^T \mathbf{M}^{-1} \mathbf{J} \mathbf{P}_k \boldsymbol{n}_k\,. \end{aligned}$$

In order to describe the single components of the different vectors and matrices, we define the matrix

$$\tilde{\boldsymbol{A}}_{lk} = \mathbf{P}_l^T \mathbf{J}^T \mathbf{M}^{-1} \mathbf{J} \mathbf{P}_k \in \mathbb{R}^{3\times 3}$$

with:

$$\begin{aligned}
\tilde{\boldsymbol{A}}_{lk} &= \delta_{i_l i_k} \left(\frac{1}{m_{i_k}} \mathbf{E} - \mathbf{r}_{li_l}^{\times} \mathbf{I}_{i_k}^{-1} \mathbf{r}_{ki_k}^{\times} \right) \\
&- \delta_{i_l j_k} \left(\frac{1}{m_{j_k}} \mathbf{E} - \mathbf{r}_{li_l}^{\times} \mathbf{I}_{j_k}^{-1} \mathbf{r}_{kj_k}^{\times} \right) \\
&- \delta_{j_l i_k} \left(\frac{1}{m_{i_k}} \mathbf{E} - \mathbf{r}_{lj_l}^{\times} \mathbf{I}_{i_k}^{-1} \mathbf{r}_{ki_k}^{\times} \right) \\
&+ \delta_{j_l j_k} \left(\frac{1}{m_{j_k}} \mathbf{E} - \mathbf{r}_{lj_l}^{\times} \mathbf{I}_{j_k}^{-1} \mathbf{r}_{kj_k}^{\times} \right) .
\end{aligned}$$

For the components of $\mathbf{A}_{00}$, $\mathbf{A}_{lk}$ and $\boldsymbol{a}_{lk}$ follows with $1 \leq l, k \leq K$ and $1 \leq i, j \leq \eta$:

$$\begin{aligned}
(\mathbf{A}_{lk})_{ij} &= \boldsymbol{d}_{li}^T \tilde{\boldsymbol{A}}_{lk} \boldsymbol{d}_{kj}, \\
(\boldsymbol{a}_{lk})_i &= \boldsymbol{d}_{li}^T \tilde{\boldsymbol{A}}_{lk} \boldsymbol{n}_k, \\
(\mathbf{A}_{00})_{lk} &= \boldsymbol{n}_l^T \tilde{\boldsymbol{A}}_{lk} \boldsymbol{n}_k .
\end{aligned}$$

The vector $\boldsymbol{b}$ is built up as sketched in figure 5:

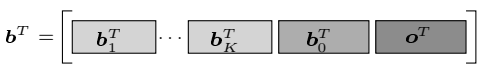

Figure 5: The structure of vector $\boldsymbol{b}$.

To determine $\boldsymbol{b}_k \in \mathbb{R}^\eta$ for $1 \leq k \leq K$ and $\boldsymbol{b}_0 \in \mathbb{R}^{\mathrm{K}}$ we use the substitution $\boldsymbol{u}^\diamond = \boldsymbol{u}^t + \Delta t \mathbf{M}^{-1} \boldsymbol{f}_{ext}$ and obtain:

$$\begin{aligned}
\boldsymbol{b}_k &= \mathbf{D}^T \mathbf{P}_k^T \mathbf{J}^T \boldsymbol{u}^\diamond, \\
\boldsymbol{b}_0 &= \mathbf{N}^T \mathbf{J}^T \boldsymbol{u}^\diamond - \frac{1}{\Delta t} \boldsymbol{\nu} .
\end{aligned}$$

Expressed component-wise with $1 \leq k \leq K$ and $1 \leq i \leq \eta$:

$$\begin{aligned}
(\boldsymbol{b}_k)_i &= \boldsymbol{d}_{ki}^T (\boldsymbol{v}_{j_k}^\diamond + \boldsymbol{r}_{kj_k} \times \boldsymbol{\omega}_{j_k}^\diamond - \boldsymbol{v}_{i_k}^\diamond - \boldsymbol{r}_{ki_k} \times \boldsymbol{\omega}_{i_k}^\diamond), \\
(\boldsymbol{b}_0)_k &= \boldsymbol{n}_k^T (\boldsymbol{v}_{j_k}^\diamond + \boldsymbol{r}_{kj_k} \times \boldsymbol{\omega}_{j_k}^\diamond - \boldsymbol{v}_{i_k}^\diamond - \boldsymbol{r}_{ki_k} \times \boldsymbol{\omega}_{i_k}^\diamond) - \frac{\nu_k}{\Delta t} .
\end{aligned}$$

In section 2.4 we explain the linearization of the contact condition and the determination of $\boldsymbol{\nu}$. This linearization requires a fixpoint-iteration for the calculation of the contact forces, which is described in the following.

2.3 How to obtain the new geometric configuration of the scene?

Up to now we described a way to determine the contact forces and torques for a given contact configuration in a virtual scene. Based on them the new linear and angular velocity of every object (using the discretized Newton-Euler equations) are determined.

LCP[..] describes the Lemke-algorithm and the crucial part of its input. Processing LCPs of order n typically requires $\mathcal{O}(n)$ pivot steps with the Lemke-algorithm. But as in the case of the simplex-algorithm there are also pathological cases that will cause the algorithm to perform an exponential number of steps. The proof of the convergence of the Lemke-algorithm is sketched in [ST95]. In our examples the iteration always converged for small enough Δt after less than five iterations. Generally we used $\Delta t \leq 10^{-3}$ and $\epsilon_{fix} \leq 10^{-4}$.

Algorithm Fixpoint-Iteration
Input: contact configuration at time t
Output: contact configuration at time $t + \Delta t$
$\boldsymbol{s}' \leftarrow \boldsymbol{s}^t + \Delta t \mathbf{S} \boldsymbol{u}^t$
repeat
  $\boldsymbol{f} \leftarrow \mathtt{LCP}(\boldsymbol{s}', \boldsymbol{u}^t)$
  $\boldsymbol{u}' \leftarrow \boldsymbol{u}^t + \Delta t \mathbf{M}^{-1} (\mathbf{J}\mathbf{N}\boldsymbol{f} + \boldsymbol{f}_{ext})$
  $\boldsymbol{s}'' \leftarrow \boldsymbol{s}'$
  $\boldsymbol{s}' \leftarrow \boldsymbol{s}^t + \Delta t \mathbf{S} \boldsymbol{u}'$
until $|\boldsymbol{s}' - \boldsymbol{s}''| < \epsilon_{fix}$
$\boldsymbol{s}^{t+\Delta t} \leftarrow \boldsymbol{s}'$

2.4 Linearization of the contact condition

The virtual objects of the GALILEO-module topologically consist of three entities: vertices, edges and faces, which are geometrically embedded in points, curves and surfaces, respectively. Following from that we distinguish four possible contact types: vertex-face, edge-edge, edge-face and face-face. With a LCP-formulation that covers in its simulation range the above contact types, all unilateral contact situations typical for VR-applications can be handled. The geometric entities of the objects (points, curves and surfaces) have a linear or a nonlinear boundary. But normally VR-objects are modeled as polyhedral shapes only and surfaces with nonlinear boundary description are simply tessellated. Then we just have vertex-face or edge-edge contacts.
The following assumption is important for all occurring contact situations:

> During the fixpoint-iteration of the algorithm the five degree-of-freedom contact constraints do not change topologically.

The global simulation time stands still during the fixpoint-iteration and there is no change of contact type because of a change in position and orientation during the iteration. We proceed in four logical steps to obtain the linearized contact-condition needed for the LCP-formalism.

2.4.1 Formulate the contact condition

For reasons of simplicity we describe the linearization for one contact point. In real applications the 'unique contact point' can only be approximated by the closest points of the two objects in contact. Let the extremal points at the k-th contact point be $\boldsymbol{p}_{i_k}$ and $\boldsymbol{p}_{j_k}$ for the objects B_{i_k} and B_{j_k}. The generalized contact configuration of these two objects is described by the 14-dimensional vector $\boldsymbol{s}_k := [\boldsymbol{c}_{i_k}, \boldsymbol{q}_{i_k}, \boldsymbol{c}_{j_k}, \boldsymbol{q}_{j_k}]^T$ with $\boldsymbol{s}_k : \mathbb{R} \to \mathbb{R}^{14},\ t \mapsto \boldsymbol{s}_k(t)$. We are interested in a distance function δ_k that determines the minimal distance of the objects B_{j_k} and B_{i_k} based on the given geometric configuration $\boldsymbol{s}_k$ at the k-th contact point: $\delta_k : \mathbb{R}^{14} \to \mathbb{R},\ \boldsymbol{s} \mapsto \delta_k(\boldsymbol{s}_k)$. The contact condition for the k-th contact point reads as:

$$\delta_k(\boldsymbol{s}_k) = \boldsymbol{n}_k^T(\boldsymbol{s}_k)(\boldsymbol{p}_{j_k}(\boldsymbol{s}_k) - \boldsymbol{p}_{i_k}(\boldsymbol{s}_k)) \geq 0 .$$

2.4.2 Use a Taylor-expansion

Because of the nonlinearity of the orientations a multidimensional Taylor-expansion around the geometric contact

configuration $\boldsymbol{s}_k^{'}$ is carried out

$$\delta_k(\boldsymbol{s}_k) \quad = \quad \delta_k(\boldsymbol{s}_k^{'}) + \left(\nabla\delta_k(\boldsymbol{s}_k^{'})\right)^T (\boldsymbol{s}_k - \boldsymbol{s}_k^{'}) + \mathcal{O}(\Delta t^2) \; .$$

2.4.3 Do a time-step

With the backwards-differentiation scheme

$$\boldsymbol{s}_k^{t+\Delta t} \quad = \quad \boldsymbol{s}_k^t + \Delta t \frac{d\boldsymbol{s}_k}{dt}(t+\Delta t) + \mathcal{O}(\Delta t^2)$$

and using the theorem of Taylor again

$$\nabla\delta_k(\boldsymbol{s}_k^{'}) \quad = \quad \nabla\delta_k(\boldsymbol{s}_k^{t+\Delta t}) + \mathcal{O}(\Delta t)$$

we obtain

$$\begin{aligned} \delta_k(\boldsymbol{s}_k^{t+\Delta t}) \quad &\doteq \quad \delta_k(\boldsymbol{s}_k^{'}) + \left(\nabla\delta_k(\boldsymbol{s}_k^{'})\right)^T (\boldsymbol{s}_k^t - \boldsymbol{s}_k^{'}) \\ &+ \quad \Delta t \left(\nabla\delta_k(\boldsymbol{s}_k^{t+\Delta t})\right)^T \frac{d\boldsymbol{s}_k}{dt}(t+\Delta t) \; . \end{aligned}$$

2.4.4 Simplify and rearrange the contact condition

With $g_k(t) := (\delta_k \circ s_k)(t) : \mathbb{R} \rightarrow \mathbb{R}$ and application of the chain-rule

$$\frac{dg_k}{dt}(t+\Delta t) \quad = \quad \left(\nabla\delta_k(\boldsymbol{s}_k^{t+\Delta t})\right)^T \frac{d\boldsymbol{s}_k}{dt}(t+\Delta t)$$

holds. According to Anitescu, Cremer and Potra [ACP95] and Montana [Mo88] the exact value for $\dot{g}_k$ can be determined for all four contact types between two differentiable entities of the objects in contact as

$$\dot{g}_k = \boldsymbol{n}_k^T(\boldsymbol{v}_{j_k} + \boldsymbol{\omega}_{j_k} \times \boldsymbol{r}_{j_k}) - \boldsymbol{n}_k^T(\boldsymbol{v}_{i_k} + \boldsymbol{\omega}_{i_k} \times \boldsymbol{r}_{i_k}) \; .$$

Therefore our linearized contact condition $\delta_k(\boldsymbol{s}_k^{t+\Delta t}) \geq 0$ is

$$\begin{aligned} & \boldsymbol{n}_k^T(\boldsymbol{v}_{j_k}^{t+\Delta t} + \boldsymbol{\omega}_{j_k}^{t+\Delta t} \times \boldsymbol{r}_{j_k}^{t+\Delta t}) \\ - \quad & \boldsymbol{n}_k^T(\boldsymbol{v}_{i_k}^{t+\Delta t} + \boldsymbol{\omega}_{i_k}^{t+\Delta t} \times \boldsymbol{r}_{i_k}^{t+\Delta t}) \\ \geq \quad & -\frac{1}{\Delta t}\left(\delta_k(\boldsymbol{s}_k^{'}) + \left(\nabla\delta_k(\boldsymbol{s}_k^{'})\right)^T (\boldsymbol{s}_k^t - \boldsymbol{s}_k^{'})\right) \\ \Leftrightarrow \quad & \boldsymbol{n}_k^T \mathbf{P}_k^T \mathbf{J}^T \boldsymbol{u}^{t+\Delta t} \geq \frac{\nu_k}{\Delta t} \; . \end{aligned}$$

The derivations in ν_k are calculated numerically. Thus for all contact points the complementarity condition, as already described in (3), holds:

$$\mathbf{N}^T \mathbf{J}^T \boldsymbol{u}^{t+\Delta t} \geq \frac{\boldsymbol{\nu}}{\Delta t} \quad \text{compl. to} \quad \boldsymbol{f} \geq \mathbf{0} \; .$$

3 An evaluation example from 'classical-mechanics'

3.1 The motivation

The GALILEO-system was designed for the solution of multi-body simulation tasks, but already the simulation of the mechanical behaviour of just one object can be quite complicated. A very famous example is the so-called tippe-top.

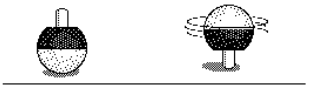

Figure 6: The classical tippe-top and its overturn.

It appears to be stable when spun slowly, but if it is spun faster it overturns and spins on its stick (see figures 6 and 8). Roughly speaking, the friction at the contact point(s) between the tippe-top and the plane is the reason for the inversion. Cohen described in [Co77] the fascination that stems from this toy with the words,

> *'The tippe top's motion constitutes the sort of phenomenon abundant in physics, for which a simple physical analysis reveals the underlying principles. Yet for which a detailed and rigorous solution (which may require the use of computing machines) is necessary to confirm the analysis.'.*

The simulation of this mechanical toy is quite a good test example for the modeling capabilities of our approach, especially concerning the simulation of frictional effects with a linearized friction model. We cannot go into the physical details of the tippe-top here and refer to the literature, but there really is a simple physical argument why the overturning motion can only be explained by considering friction forces.

Figure 7: N. Bohr and W. Pauli, the two Nobel-prize winning physicists, watching the strange motion of a tippe-top at a time its behaviour was not understood at all.

It is due to DelCampo [De55]: If during the reversal the center of mass rises, the kinetic energy decreases and the potential energy increases. The magnitudes of the angular velocity and of the angular impulse decrease. Therefore a torque must be acting. If you neglect the friction force for a moment, only the contact force or the gravitational force could produce a torque, but the angular impulse is predominant in the direction of the vertical axis. Neither

the contact nor the gravitational force can effect this impulse in a sufficient manner because their main direction is also the vertical one. Therefore another force, the friction force, must be responsible for the tipping-effect.

Classical papers are [Br52], [Hu52], [Pl54], [Sy52]. [Co77] and [Or94] carried out computer-simulations. The most important former work has been presented by Kane and Levinson [KL78]. But up to now all simulations (see the last three citations) just imitate the behaviour of an eccentric sphere by integrating the equations of motion that are adapted to the special geometry of the sphere. The results of the simulations are partly incorrect because of wrong friction modeling (see e.g. the comments of [KL78] on [Co77]).

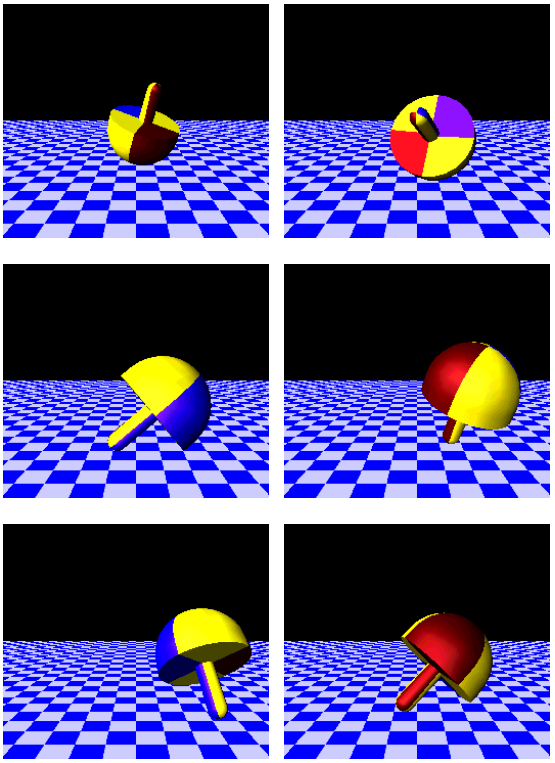

Figure 8: Some snapshots from the tippe-top simulation with the GALILEO-module of DBView. The second picture in the left column shows the tippe-top in contact with the plane at two contact points.

3.2 The simulation

We present a few results of our rigid body simulation carried out with the above constraint-based approach for the tippe-top with two contact points. See the following figures 10, 11, 12 and 13 that show a few selected simulation results. The main results are:

- The tipping-effect can be reproduced with an arbitrary number of facets in the Coulomb friction pyramid.
- Our rigid body simulations satisfy the real-time demands or at least come near to real-time depending of course on the stepsize Δt of the algorithm. For example in the simulation of the non-homogeneous sphere the following computing-times for the solution of the LCP were achieved on an SGI Infinite Reality (one R10000 processor, averaging of 10000 tests):

dimension of $\mathbf{A}$	6	10	18
time in milliseconds	0.765	1.202	2.764
dimension of $\mathbf{A}$	34	66	130
time in milliseconds	7.941	27.464	110.923

  Since $\mathbf{A} \in \mathbb{R}^{(\eta+2)\cdot \mathrm{K} \times (\eta+2)\cdot \mathrm{K}}$ holds, the dimension of $\mathbf{A}$ increases if the number of contact points grows or if the quality of the friction pyramid is improved. To obtain the above tabular we increased η, i.e. the quality of friction modeling.

- The results we obtained for the eccentric sphere simulation are identical to the results of Kane and Levinson [KL78], who performed the best simulations so far for this example.
- Beyond that we carried out the same simulations with our implementation of the impulse-based method. At the moment the impulse-based approach is the best simulation technique for one contact point situations. The result was that all the curves were 'nearly identical', even for a small number of facets in the linearized friction model.

In summary, we found the constraint-based approach showing very good performance concerning both efficiency and physical correctness.

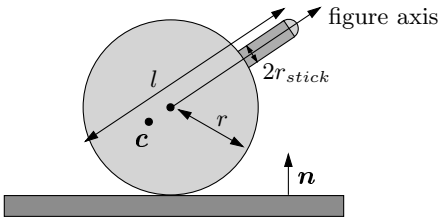

Figure 9: The specification of the tippe-top.

The geometric specification of our tippe-top, the initial dynamic configuration in the metric system and some algorithmic parameters are: $\Delta t = 10^{-4}$, $\epsilon_{fix} = 10^{-4}$, $\mu = 0.6$, $\eta = 4\ (8, 16, 32)$, radius of the sphere $r = 0.025$, radius of the spherical end of the stick $r_{Stick} = 10^{-2}$, length of the tippe-top (along the figure-axis) $l = 0.060$, $\boldsymbol{n} = [0, 1, 0]^T$, $\boldsymbol{q} = [-0.316, 0.065, -0.938, -0.126]^T$, $\boldsymbol{\omega} = [0, 150, 0]^T$, $\boldsymbol{v} = [0.1, 0.0, 0.2]^T$, $m = 0.015$, $I_{11} = I_{22} = I_{33} = 3.75 \cdot 10^{-6}$, $\boldsymbol{c} = [0.0, 0.02020, 0.0]^T$. See figure 9 for further explanation.

3.3 The modeling of rolling friction

Figure 13 shows the energy of the tippe-top during the simulation. After the inversion of the tippe-top at time $t \approx 0.6$ the energy only decreases very slowly. This problem can be resolved by introducing an approximative modeling of rolling friction. In the case of rolling friction the contact point velocity $\dot{\boldsymbol{p}}$ disappears:

$$\begin{aligned} \dot{\boldsymbol{p}} &= \boldsymbol{v} + \boldsymbol{\omega} \times \boldsymbol{r} = \boldsymbol{0} \\ \Leftrightarrow \quad \boldsymbol{v} &= \boldsymbol{r} \times \boldsymbol{\omega}\,. \end{aligned}$$

The Coulomb-law for dynamic friction determines the friction force as $\mathbf{F}_t = -\mu |\mathbf{F}_n| \frac{\dot{\boldsymbol{p}}_t}{|\dot{\boldsymbol{p}}_t|}$. Consequently from $\dot{\boldsymbol{p}} \to 0$ follows $\mathbf{F}_t \to 0$. Therefore the loss of energy is very small.

Caused by this not very realistic preservation of energy the tippe-top keeps on turning for a long time after its overturn. The Kane and Levinson approach had the same problem as well as the impulse-based approach. To solve this problem we introduced, following Lewis and Murray [LM95], two additional forces in the case of rolling-friction:

1. A modified friction force:

$$\boldsymbol{F}_t^{roll} = -\mu_R m \boldsymbol{g} \frac{\boldsymbol{v}_t}{|\boldsymbol{v}_t|}$$

   with $\mu_R = 1.0$ being a rolling friction coefficient. The velocity $\boldsymbol{v}_t$ of the center of mass in tangential direction does not vanish at the point in time the velocity of the contact point tends towards zero.

2. A simple approximative model of air resistance yielding in the following torque:

$$\boldsymbol{M}_t = -\mu_A \boldsymbol{\omega}_t$$

   with $\mu_A = 0.001$ representing an air resistance coefficient.

In the discretized Newton-Euler equation $\boldsymbol{F}_t^{roll}$ denotes the friction force at this contact point and $\boldsymbol{M}_t$ is simply added to the external forces exerted on the object. Using these two additional forces the object behaviour of the sphere is much more realistic than before. Because the new forces are always dissipative, the energy consistency of the approach (see [ST95]) still holds, although the handling of these exceptions is not integrated in the LCP-formalism of the constraint-based approach.

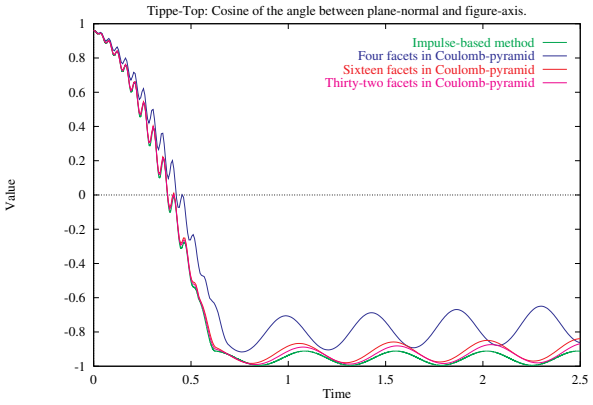

Figure 10: The cosine of the angle between the plane-normal and the figure-axis of the top shows the overturning and nutational motion of the top.

4 Summary and further work

We described the constraint-based approach to multibody problems of the GALILEO-system. This approach allows the description of the geometrical and dynamical configurations of n polyhedral and/or curved objects with K contact points under consideration of a scalable friction model in a single linear complementarity problem. The solution of this LCP using e.g. the Lemke-algorithm then delivers the contact force and the torque exerted on every object. Based on this

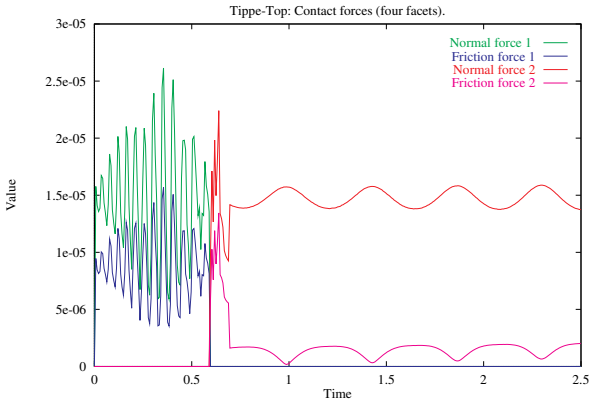

Figure 11: The contact and friction forces for the two contact points.

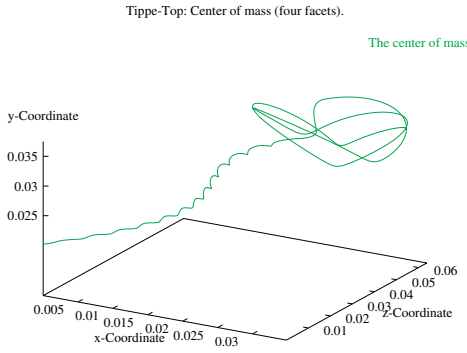

Figure 12: The lifting-motion of the center of mass.

information the new geometrical and dynamical configuration of all objects can be determined. To obtain the new configurations a fixpoint-iteration must be performed. The linearizations of the contact conditions and of the friction cone, which are necessary to obtain a linear complementarity problem, are described. Simulation and animation of multibody systems becomes more and more important in the VR-community. Physical modeling of objects helps to increase the immersion in virtual worlds very much. The GALILEO-system is a quite general VR-oriented rigid body dynamics module and is integrated as a prototype into the Daimler-Benz DBView-VR-platform.

The simulation of the classical tippe-top shows the very good friction modeling capabilities of the approach. Beyond that it is the first rigid-body simulation of this well-studied toy. Our hybrid system will be completed by defining and testing transition rules between the constraint- and the impulse-based approach. Further on we will also do simulations of other problems from the field of classical mechanics. We end with some words of Schiller, who said in his poem 'Thekla',

'There often is much sense in childish play.'.

In the case of the tippe-top this seems to be very true.

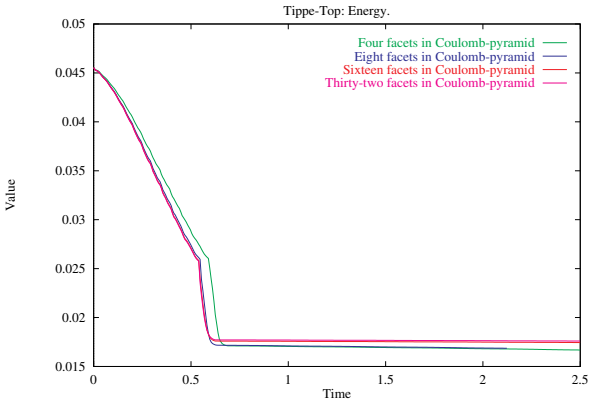

Figure 13: The energy of the tippe-top during its motion.

Acknowledgements

We thank Prof. G. Hotz, head of the Institute of Applied Mathematics and Computer Science at the Computer Science Department of the Universität des Saarlandes, for his support and his valuable comments on this ongoing research.

References

[ACP95] M. Anitescu, J. F. Cremer, F. A. Potra, Formulating 3D contact dynamics problems, *Report, Department of Mathematics, University of Iowa*, 1995

[Ba89] D. Baraff, Analytical methods for dynamic simulation of non-penentrating rigid bodies, *Proceedings of the ACM Computer Graphics Conference*, 1989

[Ba93] D. Baraff, Issues in computing contact forces for non-penetrating rigid bodies, *Algorithmica*, 1993

[Br52] C. M. Braams, On the influence of friction on the motion of a top, *Physica*, 1952

[BB88] R. Barzel, A. Barr, A modeling system based on dynamic constraints, *Proceedings of the ACM Computer Graphics Conference*, 1988

[Co77] R. J. Cohen, The tippe top revisited, *American Journal of Physics*, 1977

[CPS92] R. W. Cottle, J.-S. Pang, R. E. Stone, The linear complementarity problem, *Academic Press, Inc.*, 1992

[De55] A. R. Del Campo, Tippe top (topsy-turvey top) continued, *American Journal of Physics*, 1955

[Ha88] J. K. Hahn, Realistic animation of rigid bodies, *Proceedings of the ACM Computer Graphics Conference*, 1988

[Hu52] N. M. Hugenholtz, On tops rising by friction, *Physica*, 1952

[Ke86] J. B. Keller, Impact with friction, *Journal of Applied Mechanics*, 1986

[KL78] T. R. Kane, D. A. Levinson, A realistic solution of the symmetric top problem, *Journal of Applied Mechanics*, 1978

[LM95] A. D. Lewis, R. M. Murray, Variational principles for constrained systems: theory and experiment, *International Journal of Nonlinear Mechanics*, 1995

[Mi96] B. Mirtich, Impulse-based dynamic simulation of rigid body systems, *Ph.D.-Thesis, Berkeley*, 1996

[Mo88] D. J. Montana, The kinematics of contact and grasp, *International Journal of Robotics Research*, 1988

[Mo86] J. J. Moreau, Frottement, adhésion, lubrification, *Comptes Rendus, Serie II*, 1986

[MC94] B. Mirtich, J. Canny, Impulse-based dynamic simulation, *in K. Goldberg, D. Halperin, J. C. Latombe, R. Wilson, editors, The Algorithmic Foundations of Robotics, A. K. Peters, Boston, MA*, 1994

[MC95] B. Mirtich, J. Canny, Impulse-based simulation of rigid bodies, *Proceedings of the ACM Symposium on Interactive 3D Graphics*, 1995

[MM93] M. D. P. Monteiro-Marques, Differential inclusions in nonsmooth mechanical problems: shocks and dry friction, *Volume 9 of Progress in Nonlinear Differential Equations and their Application*, Birkhäuser-Verlag, 1993

[MW88] M. Moore, J. Wilhelms, Collision detection and response for computer animation, *Proceedings of the ACM Computer Graphics Conference*, 1988

[Or94] A. C. Or, The dynamics of a tippe top, *SIAM Journal of Applied Mathematics*, 1994

[Pl54] W. A. Pliskin, The tippe top (topsy-turvy top), *American Journal of Physics*, 1954

[St90] W. J. Stronge, Rigid body collisions with friction, *Proceedings of the Royal Society in London*, 1990

[St91] W. J. Stronge, Unraveling paradoxical theories for rigid body collisions, *Journal of Applied Mechanics*, 1991

[Sy52] J. L. Synge, On a case of instability produced by rotation, *Philosophical Magazine*, 1952

[SS98] J. Sauer, E. Schömer, Dynamiksimulation starrer Körper für Virtual Reality Anwendungen, *Proceedings of the ASIM'98*, 1998

[ST95] D. E. Stewart, J. C. Trinkle, An implicit time-stepping scheme for rigid body dynamics with inelastic collisions and Coulomb friction, *International Journal of Numerical Methods in Engineering*, submitted 1995

[WGW90] A. Witkin, M. Gleicher, W. Welch, Interactive Dynamics, *Proceedings of the ACM Computer Graphics Conference*, 1990